Quantum behavior of hydrogen-vacancy complexes in diamond

Kamil Czelej,* Marcin Roland Zemła, Piotr Śpiewak, and Krzysztof J. Kurzydłowski
Materials Design Division, Faculty of Materials Science and Engineering, Warsaw University of Technology, Wołoska 141, 02-507 Warsaw, Poland

(Received 11 July 2018; revised manuscript received 22 October 2018; published 6 December 2018)

Hydrogen plays an essential role in the growth process of artificial diamond and can easily form complexes with lattice vacancies. Despite substantial efforts to resolve the electronic structure and the ground-state properties of the hydrogen-vacancy (HV) center, the final remarks are ambiguous, while the complexes of vacancy with two and more hydrogen atoms remain unexplored. In this paper, we used spin-polarized, hybrid density-functional theory method to investigate electronic structure and magneto-optical properties of various hydrogen-vacancy clusters in diamond. Our theoretical results indicate a very strong tendency toward the formation of H_nV complexes up to four hydrogen atoms that are mostly electrically and optically active centers. One of the investigated defects introduce highly correlated electronic states that pose a challenge for density-functional theory and, therefore, require special treatment when charge- and spin-density-related properties are determined. We introduced an extended Hubbard model Hamiltonian with fully *ab initio* provided parameters to analyze the complex electronic structure of highly correlated H_2V^0 defects. The role of quantum tunneling of hydrogen in HV center and its impact on the hyperfine structure was discussed. We demonstrate that experimentally observed HV^{1-} center is similar to well-known NV^{1-}, i.e., I) it possesses triplet ^3A ground state and ^3E excited state in C_{3v} symmetry; II) the calculated zero-phonon line is 1.71 eV (1.945 eV for NV^{1-}). A detailed experimental reinvestigation based on optically detected electron paramagnetic resonance spectroscopy is suggested to verify whether the HV^{1-} center has metastable singlet shelving states between the ground and excited state triplets and, as a result, whether it may exhibit a spin-selective decay to the ground state.

DOI: 10.1103/PhysRevB.98.235111

I. INTRODUCTION

Pure diamond is transparent and diamagnetic material with a wide band gap ($E_g = 5.47$ eV) [1]. Once impurities or native point defects are introduced into the diamond lattice, they can form paramagnetic complexes that are often electrically and optically active color centers. Over the past few years, several optically active paramagnetic point defects in diamond have emerged as prime candidates to realize quantum bits and robust solid-state single-photon emitters [2–5]. The most famous nitrogen-vacancy (NV) color center [6–8] in diamond is widely regarded as a prototype defect for quantum information processing. It can be formed when mobile carbon vacancy gets trapped on substitutional nitrogen [9] and depends on the Fermi energy value, mainly the neutral (NV^0) and negative (NV^{1-}) charge states can be stabilized [5,9]. In particular, the negatively charged NV^{1-} has become a leading qubit candidate because its quantum states can be initialized, coherently manipulated, and read out with high fidelity at room temperature [10–13]. Furthermore, minimization of the ^{13}C isotope content in the grown diamond samples has led to remarkably long spin coherence times of the NV [14,15]. Nonetheless, the optical properties of this color center are significantly altered by a strong electron-phonon coupling of its excited states, causing a broad emission (∼100 nm) of which only 4% is focused in the zero phonon line (ZPL). Hydrogen is essentially the most abundant element present in the chemical vapor deposition (CVD) growth environment of synthetic diamond and under certain circumstances it can be easily incorporated into the diamond lattice, forming complexes with native defects [16]. In fact, a fingerprint of many H-related centers in CVD and natural diamonds has been identified mainly by their infrared, Raman, and optical signatures [17–20]. From the perspective of molecular chemistry, carbon and hydrogen form the C-H covalent bond with high dissociation energy of ∼3.7 eV [21]. Therefore, any native defect capable of forming the C-H bond will be an effective trap for mobile hydrogen atom. Obviously, the dangling bonds of carbon lattice vacancy have this capability and one would expect favorable formation of H_nV complexes. The most intensely investigated hydrogen- and vacancy-related center was observed in the infrared adsorption spectrum for the first time in 1959 by Charette [22]. It turned out that the sharp adsorption peaks at 3107 1/cm and 1407 1/cm can be detected in all types of diamonds, and they have been tentatively attributed to the stretching and bending modes of C-H and N-H groups [23–25]. The 3107 1/cm system was not correlated to any electron paramagnetic resonance (EPR) center, which is an indication of its nonparamagnetic ground state. At the beginning, bond-centered N-H-C defect was proposed as a plausible model of the 3107 1/cm system [26,27] but, later, more careful investigation suggested a trigonal geometry of the defect. Recently, a robust density-functional theory (DFT) calculation conducted by Goss *et al.* unambiguously assigned the 3107 1/cm absorption center to the VN_3H complex, where three

*kamil.czelej.dokt@pw.edu.pl

carbon atoms adjacent to vacancy are replaced by nitrogen and the remaining carbon dangling bond is terminated by hydrogen [28]. Surprisingly, a simple HV defect in diamond was identified much later by Glover *et al.* [29]. Using EPR measurements, they observed a new $S = 1$ paramagnetic system with C_{3v} symmetry and similar zero-field splitting to the NV center. Based on the recorded EPR data, the spin Hamiltonian parameters of the defect coupled to a single proton were determined to be $g_{\|} = 2.0034(5)$, $g_{\perp} = 2.0023(5)$, $D = \pm 2706(5)$ MHz, $|A_{\|}| = 1.10(5)$ MHz, $|A_{\perp}| = 1.95(5)$ MHz, where $g_{\|}$, D, and $A_{\|}$ are aligned with [111] crystallographic axis. A subsequent analysis of the electronic structure deduced from a linear combination of molecular orbitals led to the conclusion that the observed HV center is negatively charged. There are two very recent theoretical investigations focusing on single hydrogen-vacancy defect in diamond [30,31]. Peaker *et al.* analyzed the electronic structure and vibrational properties of HV in different charge states [30]. They were able to reproduce the experimentally observed triplet ground state of HV^{1-} in C_{3v} point group, paying attention to its similarity with NV^{1-} center. According to the study, in the case of neutral HV^0, both the doublet and quartet spin states are degenerate in energy and, hence, either can be the ground state of the defect, whereas Salustro *et al.* [31] found the ground state of HV^0 to be spin doublet. This discrepancy requires further theoretical investigation and, ultimately, experimental verification. To the best of our knowledge, the complexes of vacancy with two or more hydrogen atoms have not been considered so far and their electronic structure remains elusive. In this paper, we investigate electronic structure and magneto-optical properties of various hydrogen-vacancy clusters in diamond by means of spin-polarized, hybrid DFT. We found a significant driving force for hydrogen clustering with a single vacancy and relatively low formation energies of these defects. Besides the electronic structure calculations, we provide the magneto-optical and vibrational signals of the investigated defects for comparison with available experimental data, and to mediate future identification of yet unidentified hydrogen- and vacancy-related complexes. We used an extended Hubbard model to analyze the complex electronic structure of highly correlated H_2V^0 defects. We demonstrated that one of the investigated HV^{1-} centers is similar to well-known NV^{1-} and might be another interesting candidate for realizing quantum information processing in diamond.

II. COMPUTATIONAL DETAILS

The electronic structure calculations have been carried out using spin-polarized DFT (SP-DFT), with the projector augmented wave [32,33] method, as implemented in the VIENNA AB INITIO SIMULATION PACKAge (VASP). We applied the screened, range-separated, nonlocal hybrid functional HSE06 of Heyd, Ernzerhof, and Scuseria [34] to calculate the ground-state charge and spin densities of the system. Previous theoretical calculations indicate that HSE06 in group-IV semiconductors satisfies the generalized Koopmans' theorem [35]. Due to the error compensation between the Hartree-Fock and GGA exchange, HSE06 in diamond turned out to be nearly free of the electron self-interaction error and is capable of providing defect levels and defect-related electronic transitions within ∼0.1 eV, with respect to experiment [36]. To minimize finite-size effects, we selected a periodic, cubic supercell of $N = 512$ atoms. Such a large supercell enables the approximation of the first Brillouin zone (BZ) using Γ-point, at which the degeneracy of Kohn-Sham wave functions can be inspected. Our previous studies showed that this setup reproduces known experimental values in the case of point defects in diamond [36–39] and silicon [40]. Convergence parameters and equilibrium lattice constant were determined in a bulk calculation on primitive cell. A BZ sampling with an $8 \times 8 \times 8$ Monkhorst-Pack [41] mesh ($k_{\mathrm{MP}} = 83$) and the plane-wave cutoff energy of 520 eV assure convergence of the charge and spin densities. As a result, an equilibrium lattice parameter of $a_{\mathrm{HSE}} = 3.549$ Å, and indirect band gap of $E_g = 5.32$ eV agree well with the experimental values of $a = 3.567$ Å, $E_g = 5.48$ eV, respectively. Defects in the supercell were allowed to relax in constant volume until the Hellmann-Feynman forces acting on the atom were smaller than 0.01 eV/Å.

Formation energies of the defects (ΔH_f^q) as a function of the electron chemical potential E_F ($\mu_{e|_{T=0K}} = E_F$) in the band gap can be expressed as

$$\Delta H_f^q = E_{\mathrm{tot}}^q - \sum_i n_i \mu_i - q(E_{\mathrm{VBM}} - E_F) + \Delta E_{\mathrm{corr}}, \quad (1)$$

where the Fermi level E_F is aligned to the valence band maximum (VBM) of nondefective diamond, q stands for the charge state of a defect, E_{tot}^q is the total energy of defective supercell, and the μ_i is a chemical potential of the corresponding atoms ($i = C, H$). The μ_C value is calculated from the total energy of a perfect diamond lattice, whereas μ_H is deduced from the gas phase H_2. The last term ΔE_{corr} is the charge correction in total energy due to the defective supercell. After the electrostatic potential alignment, we applied $\frac{2}{3}$ of the monopole term of the Makov-Payne charge correction [42,43] to compute ΔE_{corr}. The adiabatic charge transition levels $E^{q|q+1}$ for a selected point defect can be calculated as follows:

$$E^{q|q+1} = \Delta H_f^q - \Delta H_f^{q+1}. \quad (2)$$

To calculate the potential energy surface (PES) of the excited states and the corresponding ZPL values, we applied the constrained DFT ΔSCF method [44] implemented in VASP code. This method allows one to determine the relaxation energy of the atomic cores upon optical excitation. We used the VASP implementation of density-functional perturbation theory to calculate the phonon spectrum of the systems. In this case, we applied the Perdew-Burke-Ernzerhof (PBE) [45] approximation in the Hamiltonian. The selection of PBE for computing the vibrational modes and frequencies is dictated by following reasons: (1) It has been demonstrated that PBE is able to accurately reproduce the experimental lattice constant of diamond, phonon spectrum, as well as their dependence on pressure and temperature [46]. In fact, the calculated Raman mode of 1336 1/cm for the perfect 512 atomic supercell is very close to the experimental value of 1332 1/cm [47]. (2) The application of nonlocal hybrid functional in this case is beyond the computational power of our facilities since we allow all atoms to vibrate, and as a result, for lower symmetry

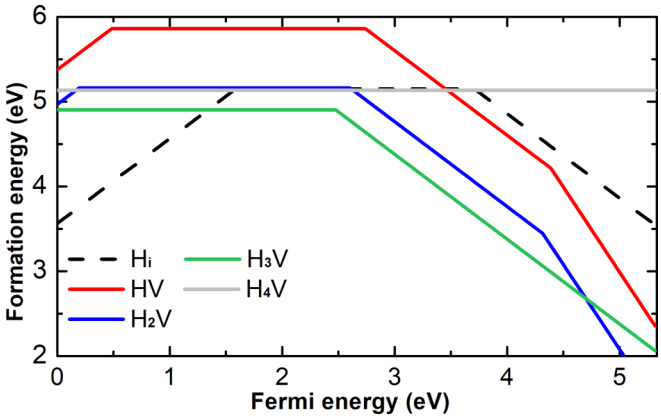

FIG. 1. Formation energy of the investigated complexes as a function of Fermi level position in the fundamental band gap of diamond. The Fermi energy level is referenced to the VBM.

defects there is >1000 vibrational degrees of freedom. To calculate the quasilocal vibrational modes with high precision, we applied very strict 10^{-4} eV/Å force convergence criterion. The normal modes were analyzed using the inverse participation ratio approach [48]. We calculated the hyperfine tensor, including the core spin polarization effect in the Fermi contact within the frozen valence approximation, using the VASP implementation suggested by Szász *et al.* [49]. In this case, the plane-wave cutoff energy was raised up to 800 eV.

III. RESULTS AND DISCUSSION

To elucidate the tendency toward the formation of hydrogen-vacancy complexes in diamond, we first analyzed binding energy of H to these complexes. In fact, we have investigated the hydrogen clustering effect on single vacancy in our previous work [36]. High positive value of H binding energy >5 eV indicates strong driving force for the entire hydrogen passivation of vacancy-related dangling bonds. The ground state geometries (see Fig. 2) of the considered HV, H_2V, H_3V, and H_4V complexes can also be found in Ref. [36]. Next, we calculated the formation energies of these defects as a function of Fermi energy level in the band gap (see Fig. 1), where the reference of the Fermi level is aligned with the VBM. From these graphs, one can predict the relative stability of a given point defect in various charge states with respect to Fermi energy level. As can be seen in Fig. 1, the HV, H_2V, and H_3V are electrically active complexes, whereas, the H_4V is entirely neutralized and does not reveal any charge transition. Interestingly, the incorporation of hydrogen atoms slightly lowers the formation energy and hence, makes the complexes even more stable. Since the H_4V defect in diamond is electrically inactive and it does not introduce any defect level in the band gap, we further focus our attention only on HV, H_2V, and H_3V.

A. Vacancy with one hydrogen atom (HV center)

When single vacancy in diamond traps a mobile hydrogen atom, one out of four carbon dangling bonds gets terminated and, as a result, HV complex is formed. According to our HSE06 results, the defect can be stabilized in positive,

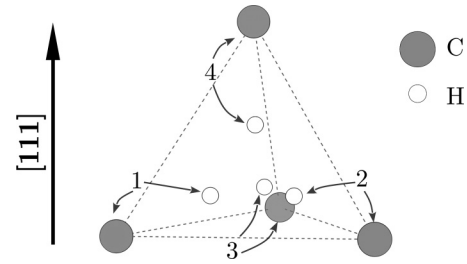

FIG. 2. The geometric sketch of H_nV center in diamond. All atoms are numerated in accordance with Table II.

neutral, negative, and doubly negative charge states. We applied the combination of group theory and the HSE06 calculated eigenvalues to describe the electronic structure of the defect (see Fig. 4). In the positive charge state that can be found only in heavily boron-doped diamond, HV has singlet ground state in C_{3v} symmetry. According to the character table of C_{3v} point group, a doubly degenerate e and nondegenerate a_1 electronic states can be constructed from symmetry adaptive basis. Only the unoccupied, doubly degenerate e state appears in the band gap while the nondegenerate a_1 falls into the valence band. By adding one electron to the empty e state, the neutral HV defect can be stabilized. This system is principally Jahn-Teller unstable and, thus, the symmetry is lowered to C_s and the former degenerate e states split into symmetric $2a'$ and antisymmetric $2a''$. Theoretically, two spin states:, doublet $S = \frac{1}{2}$ and quartet $S = \frac{3}{2}$, can be possible for HV^0. In fact, there is some controversy in literature which is the true ground state of HV^0 [30,31]. Our HSE06 calculations indicate that doublet HV^0 is more stable by 0.28 eV than quartet, supporting the conclusion reached by Salustro *et al.* [31]. As can be seen in Fig. 4, the spin electron occupies $2a''$ orbital, building up $^2A''$ many-body ground state. In principle, the electron can be promoted to $2a'$ orbital via optical excitation. Using constraint DFT method, we calculated the ZPL value for $2a'' \rightarrow 2a'$ transition and got ZPL = 1.88 eV (see Table I). Nevertheless, the excitation process associated with $2a'' \rightarrow 2a'$ transition would not generate sharp ZPL. To elucidate this statement, we constructed the sketch of adiabatic potential energy surface (APES) with respect to the atomic displacement along symmetry breaking phonon modes for different electronic states of HV^0 (see Fig. 3). If the symmetry of HV^0 is restricted to C_{3v}, it is not important which sublevel of e is occupied—both configurations $2e_x(2a')$ and $2e_y(2a'')$ must exhibit the same total energy. If the symmetry constraint is

TABLE I. The calculated zero-phonon line (ZPL) values for the selected electronic transitions.

Defect	Transition	ZPL (eV)	ZPL (eV) Ref. [30]
HV^0	$2a'' \rightarrow 2a'$	1.88	–
HV^{1-}	$a_1 \rightarrow e$	1.71	1.67
H_2V^0	$a_1 \rightarrow b_1$	2.53[a]	–
		1.49[b]	
H_2V^{1-}	$a_1 \rightarrow b_1$	0.97	–

[a]Taken from the extended Hubbard model.
[b]Taken from symmetry-restricted HSE06 ΔSCF.

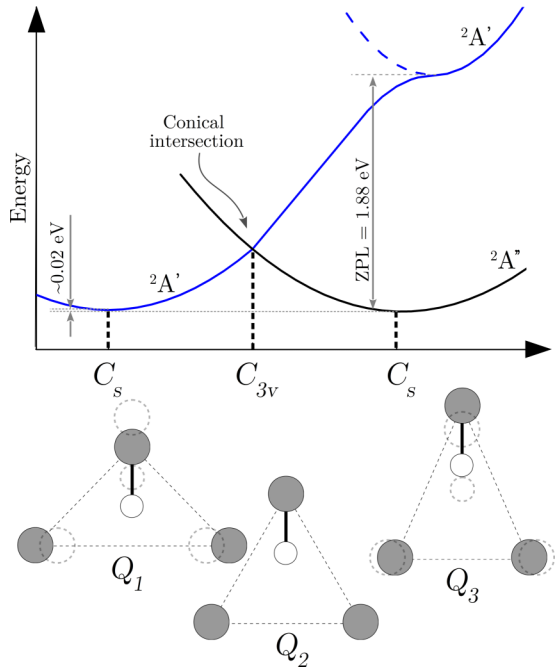

FIG. 3. Adiabatic potential energy surface of the ground and excited states of HV^0. The deformation modes of HV^0 corresponding to different electronic states are shown as well. The vertical excitation leads to $^2A'$ excited state in configuration Q_3. A metastable state (nearly degenerate in energy with the ground state) with the same type of distortion was found, which leads to an avoided crossing (the conical intersection) at C_{3v} symmetry point.

removed, the system relaxes to C_s symmetry and then the $2a''$ level is occupied by a single electron and the $2a'$ is empty. The energy from the symmetry-breaking solution is called the Jahn-Teller energy. As can be seen in Fig. 3, the C_{3v} symmetry point is the conical intersection of the Jahn-Teller effect where $2a'$ and $2a''$ levels are degenerate. The $2a'$ and $2a''$ electronic states correspond to the double layered APES of the Jahn-Teller effect. In fact, the absorption process between these two layers of the APES ($2a'' \rightarrow 2a'$) is possible with ~1.88 eV photons, but shortly afterward the system would nonradiatively relax through the conical intersection. The ~1.88 eV excitation process promotes the system to one of the vibronic excited levels. As a consequence, we suspect that there is no possible luminescent signal for HV^0 and hence, there is no sharp ZPL.To further characterize the HV^0 defect, we provide its hyperfine structure (see Table II) and quasilocal vibrational modes associated with hydrogen atom (see Table III). Based on the calculated hyperfine structure, one can notice significant coupling with three nearest ^{13}C, which is an indication of substantial spin-density localization on C-related dangling bond states. Interestingly, the hyperfine coupling with ^1H in HV^0 is one order of magnitude stronger than in HV^{1-}, which possibly makes these two charge states to be easily distinguished. We found three quasilocal vibrational modes associated with H that can be captured in infrared adsorption, Raman scattering spectrum, or phonon sideband in the photoluminescence experiment. The C-H stretching mode at 3059 1/cm belongs to a' irreducible representation of C_s point group and agrees nicely with the value of 3040 1/cm

TABLE II. Hyperfine constants of the investigated hydrogen-vacancy complexes calculated with HSE06 functional. The direction of hyperfine constants are provided in spherical coordinates [R (MHz), θ (°), φ (°)]. The θ value describes the polar angle of the [001] direction, whereas φ is the azimuthal angle of the [100] direction (on the (100) plane).

			A_{xx}			A_{yy}			A_{zz}	
	N.	R	θ	φ	R	θ	φ	R	θ	φ
HV^0 $S=\frac{3}{2}$	1 ^{13}C	25	66°	153°	25	59°	289°	45	55°	45°
	2 ^{13}C	41	114°	206°	41	45°	270°	117	55°	135°
	3 ^{13}C	41	35°	45°	41	90°	135°	117	55°	225°
	4 ^{13}C	41	66°	64°	41	135°	0°	117	126°	136°
	1 ^{1}H	9	114°	333°	9	144°	59°	13	55°	45°
HV^0 $S=\frac{1}{2}$	1 ^{13}C	27	113°	244°	13	45°	180°	10	54°	316°
	2 ^{13}C	125	75°	237°	124	40°	346°	340	54°	136°
	3 ^{13}C	125	58°	108°	124	51°	349°	340	125°	44°
	4 ^{13}C	102	114°	243°	102	45°	180°	293	55°	315°
	1 ^{1}H	52	49°	330°	16	135°	0°	36	72°	74°
HV^{1-} $S=1$	1 ^{13}C	10	114°	333°	10	142°	72°	9	125°	225°
	2 ^{13}C	89	115°	208°	89	45°	270°	175	56°	137°
	3 ^{13}C	89	37°	45°	89	90°	135°	175	53°	225°
	4 ^{13}C	89	65°	62°	89	135°	0°	175	125°	133°
	1 ^{1}H	1.56	114°	333°	1.56	75°	304°	1.03	55°	45°
	Ref. [29] ^{1}H	1.95(5)					1.95(5)			1.10(5)
H_2V^0 $S=1$	1 ^{13}C	24	121°	143°	11	119°	34°	11	45°	90°
	2 ^{13}C	24	59°	217°	11	119°	146°	11	45°	90°
	3 ^{13}C	50	45°	270°	51	66°	27°	164	55°	135°
	4 ^{13}C	50	45°	270°	51	66°	153°	164	125°	225°
	1 ^{1}H	3	135°	270°	12	114°	154°	20	125°	135°
	2 ^{1}H	3	135°	270°	12	114°	26°	20	55°	315°
H_2V^{1-} $S=\frac{1}{2}$	1 ^{13}C	11	134°	74°	10	79°	354°	9	135°	270°
	2 ^{13}C	11	46°	286°	10	84°	191°	9	135°	270°
	3 ^{13}C	256	54°	132°	128	68°	24°	129	45°	270°
	4 ^{13}C	255	126°	228°	128	68°	156°	128	45°	270°
	1 ^{1}H	15	45°	90°	2	114°	154°	14	125°	45°
	2 ^{1}H	15	45°	90°	2	114°	26°	14	55°	315°
H_3V^0 $S=\frac{1}{2}$	1 ^{13}C	18	71°	315°	6	88°	224°	6	19°	128°
	2 ^{13}C	6	77°	167°	17	48°	65°	6	45°	270°
	3 ^{13}C	18	132°	26°	6	46°	357°	6	75°	102°
	4 ^{13}C	81	48°	264°	81	118°	203°	299	125°	315°
	1 ^{1}H	26	95°	315°	24	90°	45°	22	172°	135°
	2 ^{1}H	22	84°	6°	26	45°	97°	24	134°	90°
	3 ^{1}H	26	135°	353°	24	45°	0°	22	96°	84°

reported elsewhere [30]. The remaining bending modes at 1394 1/cm and 1323 1/cm have a' and a'' characters, whereas, the later is resonant with the valence band and, hence, much less localized. The HV^0 complex can be further ionized to HV^{1-} charge state. We found 0/1− charge transition level to be at 2.75 eV with respect to VBM. The calculated ground state of the defect is triplet ^3A in C_{3v} symmetry, consistent with previous experimental observations [29] and computational predictions [30]. Two defect-related electronic states can be found in the band gap: nondegenerate, occupied a_1 and doubly degenerate, half-occupied e (see Fig. 4). Similar to the negatively charged NV center, the excitation can be triggered from the occupied a_1 to the empty e state in the spin minority channel. In fact, the calculated ZPL = 1.71 eV for $a_1 \rightarrow e$ internal transition is indeed close to experimental

TABLE III. The calculated quasilocal vibrational modes associated with H atom. $^{(2)}$ stands for doubly degenerate modes.

Defect	Mode of vibration	Symmetry label	Frequency (1/cm)
HV^0	C-H stretching	a'	3059
			3040[a]
	C-H bending	a'	1394
		a''	1323
HV^{1-}	C-H stretching	a_1	3047
			2970[a]
	C-H bending	$e^{(2)}$	1366
H_2V^0	C-H stretching	a_1	3534
		b_1	3366
	C-H bending	a_1	1551
H_2V^{1-}	C-H stretching	a_1	3344
		b_1	3137
	C-H bending	b_1	1606
H_3V^0	C-H stretching	a_1	3719
		$e^{(2)}$	3466
	C-H bending	$e^{(2)}$	1474
		a_1	1432
H_3V^{1-}	C-H stretching	a_1	3450
		$e^{(2)}$	3125
	C-H bending	$e^{(2)}$	1577
		a_1	1518

[a] Ref. [30].

1.945 eV value reported for NV^{1-} and 1.67 eV estimated for HV^{1-} by Peaker *et al.* [30]. The calculated hyperfine constants of HV^{1-} complex reproduce accurately weak coupling with ^1H observed in EPR experiment by Glover *et al.* [29]. We also calculated the quasi-local vibrational modes associated with hydrogen: C-H stretching at 3047 1/cm (a_1 character) and doubly degenerate C-H bending mode at 1366 1/cm (e character). Due to striking similarity between HV^{1-} and well-known qubit NV^{1-}, we conclude that it would be interesting to reexamine the HV^{1-} center by means of optically detected EPR spectroscopy (ODMR) to verify whether the optical polarization cycle can be achieved for the defect and, ultimately, whether it can act as a qubit similar to NV^{1-}. According to our HSE06 results, the double negative charge state of HV defect may theoretically exist in phosphorus-doped diamond. The addition of a third electron to doubly degenerate e orbital again drives the system to the lower C_s symmetry due to Jahn-Teller static effect. The electronic ground state of the defect is doublet $^2A'$ where the spin electron occupies $2a''$ orbital. In principle, there is one possible internal electronic transition $2a'' \rightarrow 2a'$ in the spin majority channel. We did not calculate the ZPL for this transition; however, we anticipate it to be within far infrared region due to small separation between $2a''$ and $2a'$ orbitals. Similar to HV^0, we anticipate the existence of conical intersection in the APES of HV^{2-} and, as a result, the fast nonradiative decay to the ground state.

B. Vacancy with two hydrogen atoms (H_2V center)

To the best of our knowledge, the complex of single vacancy with two hydrogen atoms in diamond has not been assigned yet to any known EPR or PL center. Here, we investigate the H_2V defect in detail to mediate its future identification. When two hydrogen atoms get trapped by single vacancy, two out of four C-dangling bond states get terminated and complex of C_{2v} point-group symmetry is formed. Our HSE06 calculations show that the defect may exist in positive, neutral, negative, and doubly negative charge states, whereas, the H_2V^{1+} is unlikely to be found in diamond due to its extremely narrow stability window. According to the C_{2v} character table, nondegenerate a_1, a_2, b_1, and b_2 orbitals can be constructed. We found the neutral H_2V^0 complex very challenging for standard DFT so its thorough description will be provided separately (see Sec. III D). In the negative charge state, two defect-related electronic levels appear in the band gap: the occupied a_1 and half-occupied b_1 forming paramagnetic doublet $^2B_1$ many-body ground state (see Fig. 4). There is one possible internal electronic transition $a_1 \rightarrow b_1$ in the spin

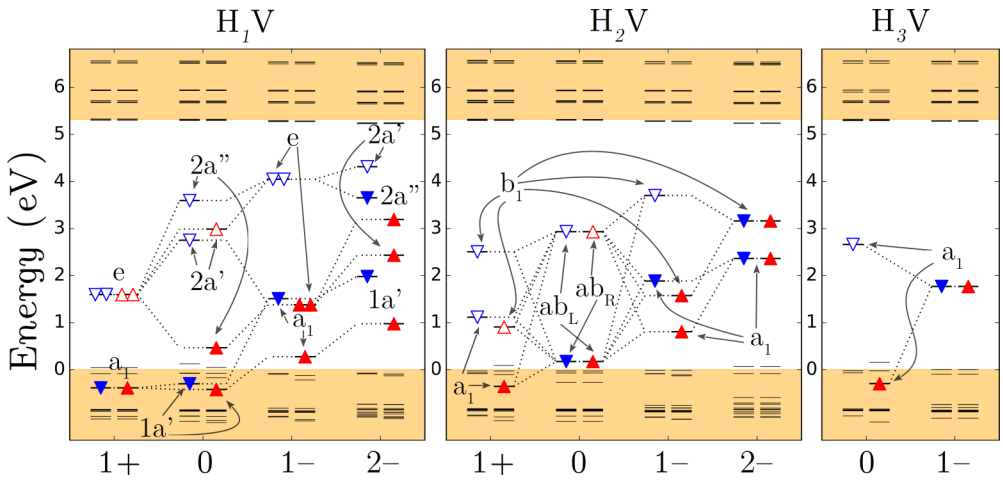

FIG. 4. Localized Kohn-Sham levels of the investigated complexes in diamond calculated with HSE06 hybrid functional. The light orange shaded area represents the conduction and valence band of an ideal diamond. Spin down (up) channels are indicated by blue (red) triangles, whereas, the filled (unfilled) triangles represent the occupied (empty) states. For the sake of clarity, the corresponding K-S states in different charge states are linked by black dotted lines.

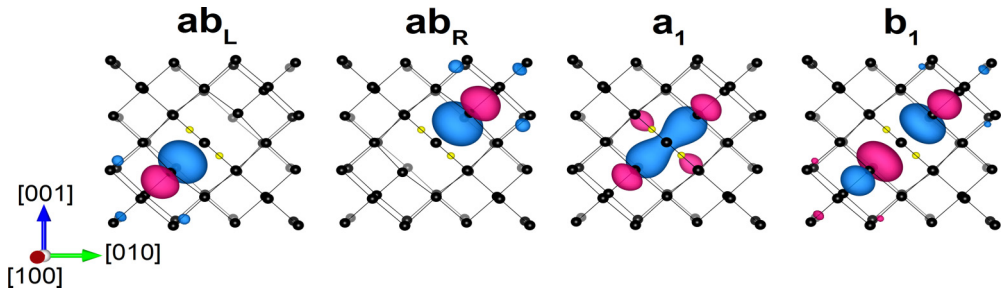

FIG. 5. 3D representation of the symmetry-broken Kohn-Sham wave functions for highly correlated H_2V^0 defect in diamond. The symmetrical a_1 and b_1 orbitals calculated for the closed-shell singlet H_2V^{2-} are also depicted. The red (blue) lobes indicate the positive (negative) phase of the wave functions with arbitrary selected isosurface value.

minority channel of H_2V^{1-} with the calculated ZPL = 0.97 eV. The calculated hyperfine coupling constants of H_2V^{1-} defect (see Table II) indicate significant spin-density localization on two C-dangling bonds. We found several quasilocal vibrational modes associated with H atom at 3344 1/cm (C-H stretching mode with a_1 character), 3137 1/cm (C-H stretching mode with b_1 character), and 1606 1/cm (C-H bending mode with a_1 character). In the doubly negative charge state, the complex has closed-shell singlet electronic configuration with both a_1 and b_1 defect orbitals filled. It is neither an optically nor EPR active center.

C. Vacancy with three hydrogen atoms (H_3V center)

Finally, we briefly analyze the complex of single vacancy with three hydrogen atoms. In this complex, three out of four C-dangling bond states are terminated by H, giving rise to C_{3v} point-group symmetry of the defect. The neutral and negative charge states were found to be feasible with the $0/1-$ adiabatic charge transition level located in the middle of the band gap (see Fig. 1). Only one nondegenerate a_1 orbital appears in the band gap, while the doubly degenerate e state falls into the valence band. The neutral H_3V^0 is paramagnetic doublet and, therefore, can be observed via EPR spectroscopy (see the hyperfine constants in Table II). We conclude that the defect does not produce any luminescence since the only possible electronic transition is from the valence band to a_1 state in the spin minority channel; however, the valence band orbitals are delocalized in nature and hole created upon optical excitation may rapidly recombine with delocalized electron, leaving behind the defect negatively charged. The negatively charged H_3V^{1-}, in turn, has closed-shell singlet electronic configuration and is optically inactive. Although the H_3V^{1-} cannot be identified via EPR measurements, it can be detected by C-H characteristic vibrations in infrared or Raman spectrum. The calculated frequencies of C-H quasilocal vibrational modes together with the corresponding symmetry labels can be found in Table III.

D. Highly correlated electronic structure of H_2V^0

To understand the electronic structure of H_2V^0 complex, one has to take into account a highly correlated nature of the defect-related orbitals in the ground state. As previously discussed by Thiering *et al.* [50], the application of HSE06 functional may lead to the symmetry-broken solution due to the presence of Fock operator. In such cases, the Kohn-Sham wave functions do not follow symmetry of defect-containing supercells and hence, they are not necessarily the eigenstates of the corresponding space group of the supercell. This is an indication of highly correlated orbitals that cannot be expressed by single Slater determinant but the exact solution is multideterminant in nature. In the case of H_2V^0, when two electrons occupy a_1 level, the electronic state can be described as singlet $^1A_1$. Nevertheless, one should realize that $b_1^{(2)}$ electron configuration also has A_1 symmetry and, hence, strong Coulomb interaction between these two electronic states might be expected. Our unrestricted SP-DFT HSE06 calculations of H_2V^0 lead to the symmetry-broken solution. As can be seen in Fig. 5, the symmetry-broken Kohn-Sham wave functions represent the C_s point group, which is lower than the C_{2v} point group of the defect itself. In this case, the spin-up and spin-down electrons are entirely localized on the "left" and "right" dangling bonds, respectively. The symmetry-restricted Kohn-Sham orbitals that truly represent the C_{2v} point group of the defect are also shown in Fig. 5. In the symmetry-broken solution, the character of a_1 and b_1 states disappears and the exact solution of many-body wave function is two-determinant open shell singlet for which the real orbitals are mixture of a_1 and b_1 states. To properly describe the electronic structure of H_2V^0 complex and the energy order of singlets and triplets, we applied an extended Hubbard model following the computational procedure proposed by Udvarhelyi *et al.* for N_2V defect [51]. Let us consider the Kohn-Sham states of the H_2V^0 depicted in Fig. 6. There are two defect-related electronic states in the band gap: the highest occupied state a_1 (HOMO) and the lowest unoccupied state b_1 (LUMO). Here, we select the HOMO and LUMO states as an active space for correlated electrons in our extended Hubbard model. For the sake of simplicity we label these two a_1 and b_1 states a and b. These states can be derived based on group theory considerations and projection operator method for symmetry adaptive linear combination of A and B dangling bond states. The explicit forms of a and b states are $a = \frac{1}{\sqrt{2}}(A + B)$ and $b = \frac{1}{\sqrt{2}}(A - B)$. Having the symmetry adaptive basis, we can express the possible many-electron states as $|^1A_{1(g)}\rangle = |a^\uparrow a^\downarrow\rangle$, $|^1A_{1(e)}\rangle = |b^\uparrow b^\downarrow\rangle$, and $|^1B_1\rangle = \frac{1}{\sqrt{2}}(|a^\uparrow b^\downarrow\rangle - |a^\downarrow b^\uparrow\rangle)$, and triplet determinants as $|^3B_1, m_s = 1\rangle = |a^\uparrow b^\uparrow\rangle$, $|^3B_1, m_s = 0\rangle = \frac{1}{\sqrt{2}}(|a^\uparrow b^\downarrow\rangle + |a^\downarrow b^\uparrow\rangle)$, $|^3B_1, m_s = -1\rangle = |a^\downarrow b^\downarrow\rangle$. The electronic structure of H_2V^0 defect may be described in Hubbard model with additional

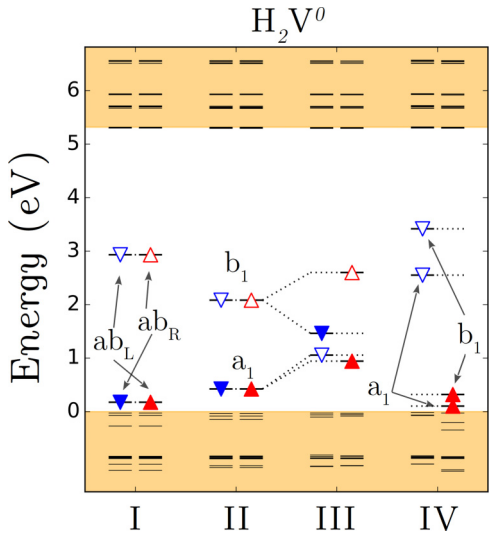

FIG. 6. HSE06 calculated electronic structure and the lowest energy excitation of highly correlated H_2V^0 defect in diamond. I represents the symmetry-broken solution, II represents the self-consistent solution with fixed symmetrical orbitals, III represents the lowest energy optical transition calculated for symmetrical orbitals, and IV represents the non-highly correlated triplet state of H_2V^0.

terms by an Hamiltonian operator expressed as

$$\hat{H} = \hat{H}_0 + \frac{U}{2}\sum_{i,\sigma}\hat{n}_{i\sigma}\hat{n}_{i\sigma'} - t\sum_{\langle i,j\rangle,\sigma}\hat{c}^{\dagger}_{i\sigma}\hat{c}_{j\sigma} + \frac{C}{2}\sum_{i,\sigma,\sigma'}\hat{n}_{i\sigma}\hat{n}_{i'\sigma'} - 2J\sum_{i}\vec{S}_i\cdot\vec{S}_{i'}, \quad (3)$$

where $\hat{c}^{\dagger}_{i\sigma}$ ($\hat{c}_{i\sigma}$) stands for a creation (annihilation) operator of an electron with spin σ ($=\uparrow,\downarrow$) at site i ($=A, B$), and $\hat{n}_{i\sigma} = \hat{c}^{\dagger}_{i\sigma}\hat{c}_{i\sigma}$. $\hat{H}_0$ is a Hamiltonian for the bath of weakly interacting electrons. Here t, U, and C represent the hopping integral, intra-, and inter-orbital direct Coulomb interactions, respectively. The Heisenberg isotropic exchange interaction with the exchange (Hund's rule) coupling of J stands in the last term. Using the symmetry adaptive basis (see Appendix A) we can write down $\hat{H}'$ ($\hat{H}' = \hat{H} - \hat{H}_0$) in matrix form:

$$H' = \begin{pmatrix} \frac{U+C+3J-4t}{2} & \frac{U-C-3J}{2} & & \\ \frac{U-C-3J}{2} & \frac{U+C+3J+4t}{2} & & \\ & & U & \\ & & & C-J \end{pmatrix}. \quad (4)$$

The zero-field splitting in the $^3B_1$ state has not been taken into account. The total energies of Ψ_1, Ψ_2, Ψ_3, and $^3B_1$ states (defined as $\langle a^{\uparrow}a^{\downarrow}|\hat{H}|a^{\uparrow}a^{\downarrow}\rangle$, $\langle a^{\uparrow}b^{\downarrow}|\hat{H}|a^{\uparrow}b^{\downarrow}\rangle$, $\langle b^{\uparrow}b^{\downarrow}|\hat{H}|b^{\uparrow}b^{\downarrow}\rangle$, $\langle a^{\uparrow}b^{\uparrow}|\hat{H}|a^{\uparrow}b^{\uparrow}\rangle$, respectively) can be calculated using HSE06 ΔSCF approach. Having the relative energies of the components, one can calculate three combined parameters t, J, and $U - C$ using the following formulas:

$$t = \frac{E(\Psi_3) - E(\Psi_1)}{4}, \quad (5)$$

$$J = \frac{E(\Psi_1) - E(\Psi_2)}{2} + t, \quad (6)$$

$$U - C = 2(E(\Psi_2) - E(^3B_1)) - J. \quad (7)$$

TABLE IV. HSE06 calculated total energies of Ψ_2, Ψ_3, and $^3B_1$ states relative to total energy of Ψ_1 for the neutral H_2V defect in diamond taken from the doubly negative H_2V basis states in the optimized geometry of the neutral H_2V by the self-consistent spin-polarized HSE06 calculation.

	Relative energy (eV)
$E(\Psi_2) - E(\Psi_1)$	0.750
$E(\Psi_3) - E(\Psi_1)$	1.617
$E(^3B_1) - E(\Psi_1)$	−0.494

The proper choice of basis set for the Hubbard Hamiltonian has to be made carefully to assure reliability of the calculated eigenvalues. As thoroughly discussed by Udvarhelyi *et al.*, [51] the basis functions selected for ΔSCF calculations have to give rise to noncorrelated orbitals without spin contamination. These two demands are satisfied by closed-shell singlet states; therefore, we selected the basis functions generated for doubly negative H_2V defect. Further clarification on the choice of proper basis set can be found in Ref. [51]. The ΔSCF calculations of Ψ_1, Ψ_3, $^3B_1$, and Ψ_2 multiplets were carried out using the wave functions generated for H_2V^{2-} defect. Such a procedure guarantees the proper symmetry and spin state of single-determinant many-body states. Based on the results summarized in Table IV, the calculated parameters in the Hubbard model are $t = 0.404$ eV, $J = 0.029$ eV, and $U - C = 2.459$ eV. Due to small value of J, the singlet-triplet coupling is weak and the $U - C$ term dominates. Having all necessary parameters in this extended Hubbard Hamiltonian determined, we can calculate the energy separation between the assumed ground state $^1A_{1(g)}$ and three remaining possible electronic states of H_2V^0 center in diamond (see Table V). The second data raw in Table V can be interpreted as vertical excitation energy, whereas the third as ZPL that essentially can be compared to experiment. Similar to Udvarhelyi *et al.* [51], the relaxation energy upon optical excitation for each excited state was roughly estimated by self-consistent spin-polarized ΔSCF calculations of Ψ_3, $^3B_1$, and Ψ_2 multiplets. We found the following values of the ionic relaxation: 0.40 eV for $^1A_{1(e)}$, 0.09 eV for $^1B_1$, and 0.09 eV for $^3B_1$. The presented Hubbard model approach for highly correlated H_2V^0 defect in diamond is leading to surprising remarks. The results indicate that the energy separation between singlet $^1A_{1(g)}$ and triplet $^3B_1$ is only 0.05 eV, which means that under thermodynamic equilibrium these two states may be degenerate in energy and either can be the ground state of H_2V^0. Also the separation between the corresponding excited singlets $^1A_{1(e)}$ and $^1B_1$ is only 0.06 eV that makes unambiguous assignment of the energy order

TABLE V. Excitation energies of the neutral H_2V defect predicted by extended Hubbard model approach.

	Excitation energy (eV)	
Electronic transition	Unrelaxed	Relaxed
$^1A_{1(g)} \rightarrow {}^3B_1$	0.13	0.05
$^1A_{1(g)} \rightarrow {}^1B_1$	2.62	2.53
$^1A_{1(g)} \rightarrow {}^1A_{1(e)}$	2.87	2.47

between them challenging. Nevertheless, assuming singlet ground state, the emission of photon should be observed at about 2.5 eV. Our detailed analysis reveals a unique electronic structure of relatively simple H_2V^0 complex in diamond and provides a remedy for coping with highly correlated defects in wide band-gap materials using parameters extracted from hybrid SP-DFT method.

E. Quantum tunneling of hydrogen atom in HV center

Quantum tunneling of H atom in the vacancy-related complexes in diamond has been already reported in the literature [52–54]. This phenomena can manifest itself in the high symmetry EPR signal of certain point defects that exhibit statically lower symmetry. The high-symmetry signal can be observed when the relative timescales of the microwave field applied to flip the electron spin in the EPR experiment are longer then the tunneling period between the symmetrically equivalent distorted structures. Following the procedure suggested by Thiering *et al*. [54], we investigate the quantum tunneling effect in HV^0 and HV^{1-} complexes in diamond. In the case of HV^0, the C_{3v} symmetry implies hydrogen atom residing on the [111] principle axis. The total energy of HV^0 in C_{3v} symmetry is 0.86 eV higher than the corresponding energy in the Jahn-Teller distorted C_s configuration. This energy, Δ_E, denotes the Jahn-Teller energy. We also determined the reorientation energy barrier between the symmetrically equivalent C_s configurations using the nudge elastic band method (NEB) and HSE06 functional. The calculated reorientation energy barrier of H in HV^0 defect is 0.65 eV, which is lower than the Jahn-Teller energy. In this Jahn-Teller system described as $E \times e$, the e vibrational modes dynamically drive the system from C_{3v} to lower C_s symmetry. As shown in Ref. [54], one can determine the tunneling rate, Γ_E, using the following formula:

$$\Gamma_E = \frac{9\kappa\Delta_E}{h}\exp\left(-\frac{6\Delta_E\lambda}{\hbar\omega_A(1+3\lambda)}\right), \tag{8}$$

$$\kappa = \left(\frac{16\lambda}{3\lambda^2+10\lambda+3}\right)^2\frac{9+54\lambda-6\lambda^3-\lambda^4}{2(9-\lambda^2)(1+3\lambda)^2}, \tag{9}$$

$$\lambda = \frac{\omega_B}{\omega_A}, \tag{10}$$

where γ_A and γ_B denote the vibrational frequencies present in the Jahn-Teller distortion as obtained in the C_s configuration. The calculated tunneling rate of H is 36 THz, which is about three orders of magnitude faster than the X band at ∼10 GHz or the Q band at ∼34 GHz used in EPR absorption measurements.

Similar analysis was applied to HV^{1-} defect. In this case, the static symmetry is C_{3v} and we can assume that H can jump between all four dangling bonds, averaging out the symmetry to T_d. This Jahn-Teller system can be described as $T \times t$ with the tunneling rate:

$$\Gamma_T = \frac{2\Delta_T}{h}\exp\left(-1.24\frac{\Delta_T}{\hbar\omega_t}\right), \tag{11}$$

where Δ_T is the Jahn-Teller energy and ω_t denotes the frequency of quasilocal vibrational mode that dynamically drives the system from T_d to lower C_{3v} symmetry. We found significantly higher ΔT value of 1.59 eV than the H reorientation barrier of 0.79 eV for HV^{1-} center. Finally, the tunneling rate, Γ_T, of 4 THz is again fast enough to influence the EPR measurements. Based on these results, both, the HV^0 and HV^{1-} defects in diamond exhibit very fast quantum tunneling effect of hydrogen that should be considered, when the hyperfine structure from the EPR is analyzed.

IV. CONCLUSION

Using spin-polarized, hybrid DFT method, we analyzed the electronic structure, electrical, and magneto-optical properties of various hydrogen single-vacancy complexes in diamond. We presented strong thermodynamic preference for the formation of H_nV clusters up to entire passivation of vacancy-related dangling bonds. To thoroughly characterize the complexes, we provided hyperfine structure, quasilocal vibrational modes and optical signatures at fully *ab inito* level. One of the investigated defects of the H_2V^0 turned out to be very challenging for standard DFT calculations due to its highly correlated electronic structure. To handle this problem, we introduced an extended Hubbard model and showed how to provide the parameters to the model based on spin-polarized HSE06 calculations. Our theoretical results confirmed that quantum tunneling of hydrogen in HV center is very fast and has to be taken into account when the EPR signals are analyzed. We concluded that the HV^{1-} center should be reinvestigated by means of optically detected EPR spectroscopy to verify whether the optical polarization cycle can be achieved for the defect and, ultimately, whether it can act as a qubit similar to NV^{1-}.

ACKNOWLEDGMENTS

This research was financially supported by the Polish National Science Centre under Contract No. 2012/05/E/ST8/03104. Computing resources were provided by High Performance Computing facilities of the Interdisciplinary Centre for Mathematical and Computational Modeling (ICM) of the University of Warsaw under Grant No. GB69-32.

APPENDIX: DETAILS CONCERNING THE APPLIED EXTENDED HUBBARD MODEL

In this section, we write down the applied formulas to obtain the presented form of the Hubbard Hamiltonian, and hence the excitation energies.

The general form of the Hubbard Hamiltonian presented in the main text as Eq. (3) can be decomposed into bath of weakly interacting electron, on-site, hopping, Coulomb repulsion, and Heisenberg exchange terms and rewritten as

$$\hat{H} = \hat{H}_0 + \hat{H}_{\text{on-site}} + \hat{H}_{\text{hopping}} + \hat{H}_{\text{Coulomb}} + \hat{H}_{\text{ex}}.$$

The eigenvalue of the first term is the total energy of the bath of weakly interacting electron (E_0). On-site and hopping parts are included in the standard Hubbard model [55] and one can

express them for A and B dangling bond states, from main text, as follows:

$$\hat{H}_{\text{on-site}} = \frac{U}{2}\sum_{i,\sigma}\hat{n}_{i\sigma}\hat{n}_{i\sigma'} = U(\hat{n}_{A\uparrow}\hat{n}_{A\downarrow} + \hat{n}_{B\uparrow}\hat{n}_{B\downarrow}), \quad \text{(A1)}$$

$$\hat{H}_{\text{hopping}} = -t\sum_{\langle i,j\rangle,\sigma}\hat{c}^{\dagger}_{i\sigma}\hat{c}_{j\sigma} = -t(\hat{c}^{\dagger}_{A\uparrow}\hat{c}_{B\uparrow} + \hat{c}^{\dagger}_{A\downarrow}\hat{c}_{B\downarrow} + \hat{c}^{\dagger}_{B\uparrow}\hat{c}_{A\uparrow} + \hat{c}^{\dagger}_{B\downarrow}\hat{c}_{A\downarrow}). \quad \text{(A2)}$$

The Coulomb repulsion for H_2V^0 is

$$\hat{H}_{\text{Coulomb}} = \frac{C}{2}\sum_{i,\sigma,\sigma'}\hat{n}_{i\sigma}\hat{n}_{i'\sigma'} = C(\hat{n}_{A\uparrow}\hat{n}_{B\uparrow} + \hat{n}_{A\uparrow}\hat{n}_{B\downarrow} + \hat{n}_{A\downarrow}\hat{n}_{B\uparrow} + \hat{n}_{A\downarrow}\hat{n}_{B\downarrow}). \quad \text{(A3)}$$

The scalar product in the last term of the Hamiltonian one can rewrite in terms of the shift operators:

$$\vec{S}_i\cdot\vec{S}_j = \hat{S}^i_x\hat{S}^j_x + \hat{S}^i_y\hat{S}^j_y + \hat{S}^i_z\hat{S}^j_z = \frac{\hat{S}^i_+\hat{S}^j_- + \hat{S}^i_-\hat{S}^j_+}{2} + \hat{S}^i_z\hat{S}^j_z, \quad \text{(A4)}$$

where $\hat{S}^i_{+(-)} = \hat{c}^{\dagger}_{i\uparrow(\downarrow)}\hat{c}_{i\downarrow(\uparrow)}$, $\hat{S}^i_z = \frac{\hat{n}_{i\uparrow}-\hat{n}_{i\downarrow}}{2}$ and then the Heisenberg isotropic exchange interaction one can formulate as

$$\hat{H}_{\text{ex}} = -2J\sum_i\vec{S}_i\cdot\vec{S}_{i'} = -2J(\hat{c}^{\dagger}_{A\uparrow}\hat{c}_{A\downarrow}\hat{c}^{\dagger}_{B\downarrow}\hat{c}_{B\uparrow} + \hat{c}^{\dagger}_{A\downarrow}\hat{c}_{A\uparrow}\hat{c}^{\dagger}_{B\uparrow}\hat{c}_{B\downarrow}) - J(\hat{n}_{A\uparrow}\hat{n}_{B\uparrow} - \hat{n}_{A\uparrow}\hat{n}_{B\downarrow} - \hat{n}_{A\downarrow}\hat{n}_{B\uparrow} + \hat{n}_{A\downarrow}\hat{n}_{B\downarrow}). \quad \text{(A5)}$$

The three-singlet and one-triplet states described in the main text formulated in terms of a and b orbitals can be expressed in terms of dangling bond states as

TABLE VI. Matrix elements of the extended Hubbard Hamiltonian acting on symmetry adaptive basis in dangling bonds representation.

	$\lvert A^{\uparrow}A^{\downarrow}\rangle$	$\lvert A^{\uparrow}B^{\uparrow}\rangle$	$\lvert A^{\uparrow}B^{\downarrow}\rangle$	$\lvert A^{\downarrow}B^{\uparrow}\rangle$	$\lvert A^{\downarrow}B^{\downarrow}\rangle$	$\lvert B^{\uparrow}B^{\downarrow}\rangle$
$\langle A^{\uparrow}A^{\downarrow}\rvert$	U	0	$-t$	t	0	0
$\langle A^{\uparrow}B^{\uparrow}\rvert$	0	$C-J$	0	0	0	0
$\langle A^{\uparrow}B^{\downarrow}\rvert$	$-t$	0	$C+J$	$-2J$	0	$-t$
$\langle A^{\downarrow}B^{\uparrow}\rvert$	t	0	$-2J$	$C+J$	0	t
$\langle A^{\downarrow}B^{\downarrow}\rvert$	0	0	0	0	$C-J$	0
$\langle B^{\uparrow}B^{\downarrow}\rvert$	0	0	$-t$	t	0	U

$$|^1A_{1(g)}\rangle = \tfrac{1}{2}(|A^{\uparrow}A^{\downarrow}\rangle + |A^{\uparrow}B^{\downarrow}\rangle + |B^{\uparrow}A^{\downarrow}\rangle + |B^{\uparrow}B^{\downarrow}\rangle), \quad \text{(A6)}$$

$$|^1A_{1(e)}\rangle = \tfrac{1}{2}(|A^{\uparrow}A^{\downarrow}\rangle - |A^{\uparrow}B^{\downarrow}\rangle - |B^{\uparrow}A^{\downarrow}\rangle + |B^{\uparrow}B^{\downarrow}\rangle), \quad \text{(A7)}$$

$$|^1B_1\rangle = \frac{1}{\sqrt{2}}(|A^{\uparrow}A^{\downarrow}\rangle - |B^{\uparrow}B^{\downarrow}\rangle), \quad \text{(A8)}$$

$$|^3B_1, m_s = 1\rangle = |A^{\uparrow}B^{\uparrow}\rangle, \quad \text{(A9)}$$

$$|^3B_1, m_s = 0\rangle = \frac{1}{\sqrt{2}}(|B^{\uparrow}A^{\downarrow}\rangle - |A^{\uparrow}B^{\downarrow}\rangle), \quad \text{(A10)}$$

$$|^3B_1, m_s = -1\rangle = |A^{\downarrow}B^{\downarrow}\rangle. \quad \text{(A11)}$$

Then one can calculate the excitation energies as an energy difference between eigenvalues of presented Hubbard Hamiltonian, which are

$$E(^1A_{1(g)}) = E_0 + \frac{C+3J+U}{2} \frac{-\sqrt{4t^2+(C-U+3J)^2}}{2}, \quad \text{(A12)}$$

$$E(^1A_{1(e)}) = E_0 + \frac{C+3J+U}{2} \frac{+\sqrt{4t^2+(C-U+3J)^2}}{2}, \quad \text{(A13)}$$

$$E(^1B_1) = E_0 + U, \quad \text{(A14)}$$

$$E(^3B_1) = E_0 + C - J. \quad \text{(A15)}$$

[1] C. J. H. Wort and R. S. Balmer, Mater. Today **11**, 22 (2008).
[2] C. Kurtsiefer, S. Mayer, P. Zarda, and H. Weinfurter, Phys. Rev. Lett. **85**, 290 (2000).
[3] D. A. Simpson, E. Ampem-Lassen, B. C. Gibson, S. Trpkovski, F. M. Hossain, S. T. Huntington, A. D. Greentree, L. C. L. Hollenberg, and S. Prawer, Appl. Phys. Lett. **94**, 203107 (2009).
[4] I. Aharonovich, S. Castelletto, D. A. Simpson, C. H. Su, A. D. Greentree, and S. Prawer, Rep. Prog. Phys. **74**, 076501 (2011).
[5] J. R. Weber, W. F. Koehl, J. B. Varley, A. Janotti, B. B. Buckley, C. G. Van de Walle, and D. D. Awschalom, Proc. Natl. Acad. Sci. USA **107**, 8513 (2010).
[6] V. Dobrovitski, G. Fuchs, A. Falk, C. Santori, and D. Awschalom, Annu. Rev. Condens. Matter Phys. **4**, 23 (2013).
[7] G. Davies and M. F. Hamer, Proc. R. Soc. A **348**, 285 (1976).
[8] J. Wrachtrup, F. Jelezko, B. Grotz, and L. McGuinness, MRS Bull. **38**, 149 (2013).
[9] P. Deák, B. Aradi, M. Kaviani, T. Frauenheim, and A. Gali, Phys. Rev. B **89**, 075203 (2014).
[10] M. V. Gurudev Dutt, L. Childress, L. Jiang, E. Togan, J. Maze, F. Jelezko, A. S. Zibrov, P. R. Hemmer, and M. D. Lukin, Science **316**, 1312 (2007).
[11] P. Neumann, N. Mizuochi, F. Rempp, P. Hemmer, H. Watanabe, S. Yamasaki, V. Jacques, T. Gaebel, F. Jelezko, and J. Wrachtrup, Science **320**, 1326 (2008).
[12] Y. Ping, B. W. Lovett, S. C. Benjamin, and E. M. Gauger, Phys. Rev. Lett. **110**, 100503 (2013).

[13] M. W. Doherty, C. A. Meriles, A. Alkauskas, H. Fedder, M. J. Sellars, and N. B. Manson, Phys. Rev. X **6**, 041035 (2016).
[14] G. Balasubramanian, P. Neumann, D. Twitchen, M. Markham, R. Kolesov, N. Mizuochi, J. Isoya, J. Achard, J. Beck, J. Tissler, V. Jacques, P. R. Hemmer, F. Jelezko, and J. Wrachtrup, Nat. Mater. **8**, 383 (2009).
[15] K. Ohashi, T. Rosskopf, H. Watanabe, M. Loretz, Y. Tao, R. Hauert, S. Tomizawa, T. Ishikawa, J. Ishi-Hayase, S. Shikata, C. L. Degen, and K. M. Itoh, Nano Lett. **13**, 4733 (2013).
[16] J. Stiegler, J. Michler, Y. Von Kaenel, E. Blank, A. Bergmaier, and G. Dollinger, Diam. Relat. Mater. **7**, 193 (1998).
[17] B. Dischler, *Handbook of Spectral Lines in Diamond: Volume 1: Tables and Interpretations* (Springer Science & Business Media, Berlin, 2012), pp. 1–467.
[18] A. M. Zaitsev, *Book* (Springer Science & Business Media, 2001).
[19] E. Fritsch, T. Hainschwang, L. Massi, and B. Rondeau, New Diamond Front. Carbon Technol. **17**, 63 (2007).
[20] G. S. Woods and A. T. Collins, J. Phys. Chem. Solids **44**, 471 (1983).
[21] T. L. Cottrell, *The Strengths of Chemical Bonds* (Butterworths Scientific Publications, London, 1954), p. 273.
[22] J. Charette, Physica **25**, 1303 (1959).
[23] J. Charette, Physica **27**, 1061 (1961).
[24] R. M. Chrenko, R. S. McDonald, and K. A. Darrow, Nature **213**, 474 (1967).
[25] W. Runciman and T. Carter, Solid State Commun. **9**, 315 (1971).
[26] J. P. Goss, R. Jones, M. I. Heggie, C. P. Ewels, P. R. Briddon, and S. Öberg, Phys. Rev. B **65**, 115207 (2002).
[27] J. Chevallier, F. Jomard, Z. Teukam, S. Koizumi, H. Kanda, Y. Sato, A. Deneuville, and M. Bernard, Diamond Relat. Mater. **11**, 1566 (2002).
[28] J. P. Goss, P. R. Briddon, V. Hill, R. Jones, and M. J. Rayson, J. Phys.: Condens. Matter **26**, 145801 (2014).
[29] C. Glover, M. E. Newton, P. M. Martineau, S. Quinn, and D. J. Twitchen, Phys. Rev. Lett. **92**, 135502 (2004).
[30] C. V. Peaker, J. P. Goss, P. R. Briddon, A. B. Horsfall, and M. J. Rayson, Phys. Status Solidi A **212**, 2431 (2015).
[31] S. Salustro, F. S. Gentile, P. D'Arco, B. Civalleri, M. Rérat, and R. Dovesi, Carbon **129**, 349 (2018).
[32] P. E. Blöchl, Phys. Rev. B **50**, 17953 (1994).
[33] G. Kresse and D. Joubert, Phys. Rev. B **59**, 1758 (1999).
[34] J. Heyd, G. E. Scuseria, and M. Ernzerhof, J. Chem. Phys. **118**, 8207 (2003).
[35] S. Lany and A. Zunger, Phys. Rev. B **80** (2009).
[36] K. Czelej and P. Śpiewak, MRS Adv. **2**, 309 (2017).
[37] K. Czelej, K. Ćwieka, P. Śpiewak, and K. Kurzydłowski, J. Mater. Chem. C **6**, 5261 (2018).
[38] K. Czelej, P. Śpiewak, and K. Kurzydłowski, Diamond Relat. Mater. **75**, 146 (2017).
[39] K. Czelej, P. Śpiewak, and K. J. Kurzydłowski, MRS Adv. **1**, 1093 (2016).
[40] P. Śpiewak and K. J. Kurzydłowski, Phys. Rev. B **88**, 195204 (2013).
[41] H. Monkhorst and J. Pack, Phys. Rev. B **13**, 5188 (1976).
[42] G. Makov and M. C. Payne, Phys. Rev. B **51**, 4014 (1995).
[43] S. Lany and A. Zunger, Phys. Rev. B **78**, 235104 (2008).
[44] A. Gali, E. Janzén, P. Deák, G. Kresse, and E. Kaxiras, Phys. Rev. Lett. **103**, 186404 (2009).
[45] J. P. Perdew, K. Burke, and M. Ernzerhof, Phys. Rev. Lett. **77**, 3865 (1996).
[46] T. A. Ivanova and B. N. Mavrin, Phys. Solid State **55**, 160 (2013).
[47] R. J. Nemanich and S. A. Solin, Phys. Rev. B **20**, 392 (1979).
[48] J. Zhang, C. Z. Wang, Z. Z. Zhu, and V. V. Dobrovitski, Phys. Rev. B **84**, 035211 (2011).
[49] K. Szász, T. Hornos, M. Marsman, and A. Gali, Phys. Rev. B **88**, 075202 (2013).
[50] G. Thiering and A. Gali, Phys. Rev. B **92**, 165203 (2015).
[51] P. Udvarhelyi, G. Thiering, E. Londero, and A. Gali, Phys. Rev. B **96**, 155211 (2017).
[52] A. Kerridge, A. H. Harker, and A. M. Stoneham, J. Phys.: Condens. Matter **16**, 8743 (2004).
[53] M. J. Shaw, P. R. Briddon, J. P. Goss, M. J. Rayson, A. Kerridge, A. H. Harker, and A. M. Stoneham, Phys. Rev. Lett. **95**, 105502 (2005).
[54] G. Thiering and A. Gali, Phys. Rev. B **94**, 125202 (2016).
[55] J. Hubbard, Proc. R. Soc. London, Ser. A **276**, 238 LP (1963).